VNU Journal of Science: Mathematics – Physics, Vol. 38, No. 4 (2022) 76-84

VNU Journal of Science: Mathematics - Physics

Journal homepage: https://js.vnu.edu.vn/MaP

Original Article

Synthesis and Properties of Fe-Ni Nanoparticles

Dao Thi Thuy Nguyet[1], To Thanh Loan[1],
Nguyen Phuc Duong[1], Le Tuan Tu[2], Luong Ngoc Anh[1,*]

[1]*International Training Institute for Material of Science (ITIMS),*
Hanoi University of Science and Technology (HUST), 1 Dai Co Viet, Hai Ba Trung, Hanoi, Vietnam
[2]*VNU University of Science, 334 Nguyen Trai, Thanh Xuan, Hanoi, Vietnam*

Received 18 June 2022
Revised 20 July 2022; Accepted 20 July 2022

Abstract: In this work, we report a simple method to prepare the Fe-Ni alloy nanoparticles by reducing $NiFe_2O_4$ spinel ferrite nanoparticles at 600 °C in a hydrogen atmosphere. Structural analyses of the Fe-Ni alloy by XRD diffraction showed that the alloy sample is a complete single phase after the deoxidizing time of 12 hours. Field effect scanning electron microscopy (FESEM) images showed microstructure with particle sizes at the nanometer scale. The valence state of the iron ion was determined from X-ray absorption near edge spectroscopy (XANES), showing that the sample had completely Fe^o. Magnetic curves of Fe-Ni alloy nanoparticles were studied by vibrating sample magnetometer (VSM) at temperatures from 88 K to 900 K from that the technical saturation magnetization M_s and magnetic order temperature T_C were determined. The magnetoresistance effect *MR* of Fe-Ni alloy nanoparticles was also studied which is related to the tunneling of conduction electrons via grain boundaries. The obtained results of the work proved that this synthesis method is a facile, effective, and low-cost route that can be used to prepare Fe-Ni alloy nanoparticles.

Keywords: Fe-Ni alloy nanoparticles, magnetic properties, magnetoresistance, deoxidization

1. Introduction

Alloy nanoparticles are of interest for research because of their special properties at the nanometer scale, such as quantum effects, surface effects, and advantageous properties. Bimetallic nanoparticles are widely used in their practical applications for catalysis, magnetic recording, magnetic fluids, and

* Corresponding author.
E-mail address: anh.luongngoc@hust.edu.vn

https//doi.org/10.25073/2588-1124/vnumap.4739

biomedical applications. Bimetallic alloy nanoparticles can be prepared by many methods, such as mechanical milling, chemical, physical, and sol-gel [1-5]. With bimetallic alloys, the phase structure of the alloy is influenced by atomic arrangement in the crystal lattice. The atoms of two components of metallic elements can distribute randomly or preferentially in the crystal lattice, and then the alloy has a metastable disordered or an equilibrium ordered phase structure, respectively. In general, a different phase structure may affect the property and application of alloy nanoparticles. Fe-Pt alloy nanoparticles with an $L1_0$ equilibrium ordered phase structure has potential applications in ultrahigh-density magnetic recording media field due to its high coercive force but Fe-Pt alloy nanoparticles with a metastable disordered phase structure cannot be used in ultrahigh-density magnetic recording media field because the coercive force is very small [6]. The catalytic properties of Cu-Pd alloy nanoparticles with an equilibrium ordered phase structure is superior to that of alloys with a metastable disordered phase [7]. Therefore, the preparation of alloy nanoparticles with an equilibrium ordered phase structure may have significant importance in the designing and application of alloy nanoparticles. Fe-Ni alloy has been used as a soft magnet because of its excellent ferromagnetic properties [8]. In addition, Fe-Ni alloy can also be used as a catalyst in fuel cells [9], the decomposition of hydrocarbon gases, and the synthesis of carbon products [10]. At the nanometer scale, Fe-Ni alloys have other applications such as magnetic shielding [11], magnetic refrigeration [12], and catalysis [13]. The Fe-Ni alloys show superparamagnetic behavior at room temperature if the grain size of the alloys is smaller than a critical value. If the particle size is smaller than the critical size, superparamagnetic will appear [14]. The development of efficient, low-cost, and stable catalysts to further improve the kinetic properties under moderate conditions is therefore important for the practical application of these alloys. Jun-Min Yan et al., generated $Fe_{1-x}Ni_x$ (x = 0-1) nanoparticles using hydrogen catalyst from NH_3BH_3 solution at temperatures and pressures that typically show alloy nanoparticle components at sizes below 10 nm have potential applications for fuel cells and electrochemical sensors [15]. The copper dispersion method for making Fe-Ni alloys is the simplest and most common way to synthesize Fe-Ni catalysts in which a solution containing metal precursors is used to make Fe-Ni alloy as a catalyst [16-18]. With this method, the composition of Ni and Fe can be changed by varying the concentration of the precursor solutions. However, the obtained Fe-Ni nanoparticles are not uniform in composition [19].

In this work, we presented the synthesis, as well as structural, magnetic and magnetoresistance properties of Fe-Ni alloy nanoparticles using a simple deoxidization method from $NiFe_2O_4$ spinel ferrite under hydrogen and elevated temperature. Through this procedure, the nickel ferrite nanoparticles were synthesized by the sol-gel method and then thermally annealed in hydrogen gas.

2. Experimental

The synthesis of Fe-Ni alloy nanoparticles consists of two steps. In the first step, we prepared nickel ferrite nanoparticles using the sol-gel method [20]: Stoichiometric amounts of $Ni(NO_3)_2$, and $Fe(NO_3)_3$ were dissolved completely in deionized water. In these processes, the $[Ni^{2+}]$:$[Fe^{3+}]$ ration was chosen as 1:2. Each aqueous solution containing Ni^{2+} and Fe^{3+} was poured into citric acid with the total cations: citric acid molar ratio equal to 1:1. Ammonium hydroxide (NH_4OH) in aqueous form was added to the mixed solutions and the pH of the solutions was adjusted to about 10. The mixtures were stirred at 600 r/min and slowly evaporated at 90 °C to form gels. The gels were dried at 120 °C for 24 h and then heated in air at 350 °C for 2 h to form xerogels. The $NiFe_2O_4$ ferrite samples were obtained after sintering the products at 700 °C in the air for 2 h. In the second step, $NiFe_2O_4$ samples were further deoxidized at 600 °C in a hydrogen atmosphere with a constant flow of 100 ml/h for 7 h

and 12 h. The samples morphologies were observed by field emission scanning electron microscopy (FESEM, JEOL 7600, Japan), the microstructures of Fe-Ni nanoparticles were studied on the X-ray diffraction spectrum (XRD) and X-ray Absorption Near Edge Spectrum (XANES). A vibrating sample magnetometer (VSM) was used to investigate the magnetic properties and magnetoresistance of the samples. The four-probe method is used to measure resistance in an external magnetic field from 0 to 9.6 kOe at 88 K and room temperature. For the electrical measurements, the sample was pressed into a pellet with a diameter of 10 mm and a thickness of 1 mm.

3. Results and Discussion

Figure 1 shows XRD patterns of the $NiFe_2O_4$ sample synthesized by the sol-gel method and the samples after being deoxidized for 7 h and 12 h. For $NiFe_2O_4$, the results show that the sample exhibited a single crystalline phase. All the observed diffraction peaks (blue pattern) can be unambiguously indexed to the standard spinel $NiFe_2O_4$ with a cubic structure (JCPDS card no. 54-0964), and they correspond to the (200), (311), (400), (422), (511) and (440) planes, respectively.

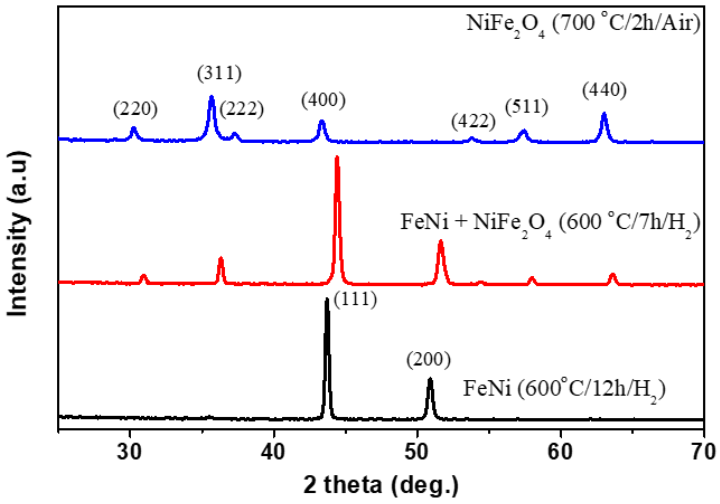

Figure 1. XRD patterns of $NiFe_2O_4$, Fe-Ni + $NiFe_2O_4$ annealed at 600 °C/7 h/H_2 and Fe-Ni annealed at 600 °C/12 h/H_2.

For the $NiFe_2O_4$ sample that was hydrogen deoxidized at 600 °C for 7 h, it is clearly found that the diffraction peaks of $NiFe_2O_4$ are weakened, but some new diffraction peaks emerged which can be identified as that the peaks of Fe-Ni alloy. The peaks included planes of the *fcc* Fe-Ni alloy and of the *bcc* Fe-Ni alloy. The sample was annealed at 600 °C for h, therefore is a mixture of the cubic $NiFe_2O_4$, *fcc* Fe-Ni, and *bcc* Fe-Ni. When the deoxidization time is up to 12 h, the peaks of *fcc* Fe-Ni strengthen further, but the peaks of *bcc* Fe-Ni disappear. Therefore, the sample as-deoxidized for 12 h is a pure *fcc* Fe-Ni alloy. Showing from the phase transformation from $NiFe_2O_4$ to Fe-Ni, one can conclude that the cubic $NiFe_2O_4$ is deoxidized to *bcc* Fe-Ni at first, then transformed into *fcc* Fe-Ni with increase of the deoxidization time. Using Debye-Scherrer formula, the average grain sizes (D) of *fcc* Fe-Ni alloy in $NiFe_2O_4$, and Fe-Ni alloy nanoparticles were estimated, it is about 25 nm and 40 nm, respectively.

This indicates that the as-deoxidized *fcc* Fe-Ni alloy grains gradually growed with the increase of deoxidization time.

The XANES spectra of the Fe-Ni alloy sample annealed in hydrogen at 600 °C for 12 h and the standard sample are shown in Fig. 2 at the *K*-edge. The oxidation state of iron ions in Fe-Ni alloy nanoparticles was determined by comparing the absorption edge energy with that of the standard Fe and FeO samples. In general, the higher the oxidation state, the larger the chemical shift of the absorption edge.

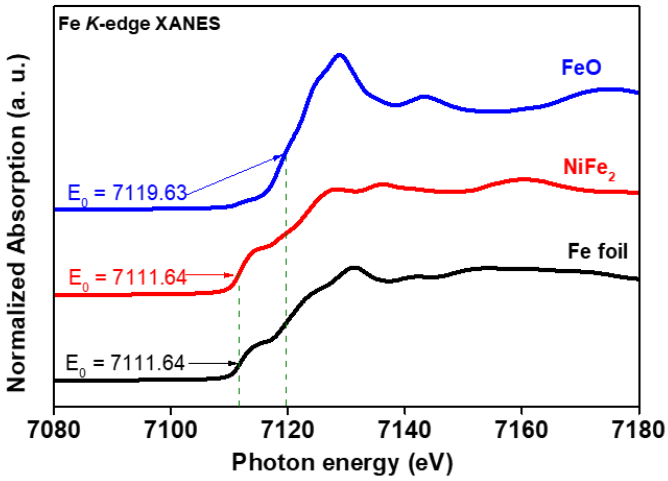

Figure 2. The Fe K-edge XANES spectra of Fe-Ni nanoparticles annealed at 600 °C/12 h/H_2 and the standard samples (iron foil and FeO).

The edge energy of the Fe-Ni alloy nanoparticles sample practically corresponds to the one of FeO, hence the oxidation state of iron in this sample is +2. The value of E_0 absorbed shore energy of the samples was determined by XANES spectrum analysis using ATHENA software [21]. The obtained results show that the absorbed shore energy value of the Fe-Ni alloy nanoparticles sample is E_0 = 7111.64 eV smaller than 7119.63 eV, the E_0 value of the FeO (Fe^{2+}) sample and equal to the value of the iron foil (Fe) sample. This proves that Fe-Ni alloy nanoparticles possess zero oxidation state, so the oxygen ions have been completely reduced in the $NiFe_2O_4$ nanoparticles.

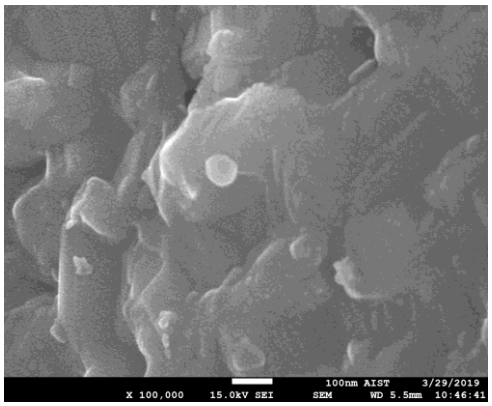

Figure 3. FESEM image of Fe-Ni nanoparticles annealed at 600 °C/12 h/H_2.

The morphology of the Fe-Ni alloy nanoparticles sample was examined by FESEM. As presented in Fig. 3, the results indicate that the particles are agglomerated in clusters of about hundreds of nanometers. However, a few discrete Fe-Ni nanoparticles with a diameter of several tens of nanometers that were determined by Debye-Scherrer formula.

In order to ascertain the presence of the magnetic phase in the compositions, isothermal magnetization measurements (*M-H*) were carried out. The magnetization loops were measured for pressed pellets samples at different temperatures from 88 K to the magnetic ordering temperature and in applied magnetic fields up to 9.6 kOe. Figure 4 shows the hysteresis loops at T = 88 K, 300 K, 540 K, and 780 K. A common feature of these loops is that they are not yet saturated in the applied fields up to 9.6 kOe. It is well known that soft magnetic materials such as Ni-Fe alloys have very low crystalline anisotropy hence their magnetizations are easily saturated in the low applied fields. In general, the superparamagnetic phenomenon occurs in ultrafine nanoparticles when the particle volume V decreases below a certain limit. The potential barrier for a fixed magnetization direction of a magnetic particle is determined as K_uV with K_u being the anisotropic density constant. If the thermal energy overcomes the potential barrier, namely $K_uV \leq 25\ kT$, where k and T are Boltzmann constant and absolute temperature, the magnetic particle turns into a superparamagnetic state. Bozorth et al., [22] showed that for Ni-Fe alloy with 33 at% nickel, the crystalline anisotropy is negligible. Based on this fact and on the shape of the magnetization curves, it is expected that the sample in our work is in the superparamagnetic state even at low temperatures.

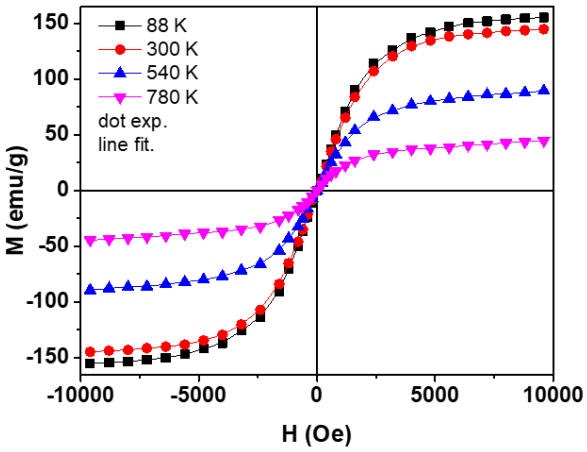

Figure 4. The hysteresis loops of the Fe-Ni sample at T=88 K, 300 K, 540 K and 780 K are fit according to the modified Langevin function (Eq. (1)).

The magnetization curves above 100 Oe can be well-fitted to the modified Langevin function.

$$M(T,H) = M_s(T)\left(cth\left(\frac{\mu H}{k_B T}\right) - \frac{k_B T}{\mu H}\right) + \chi H \quad (1)$$

where μ is the magnetic moment per particle volume and χ represents the high-field susceptibility which is usually observed in ferro/ferrimagnetic ultrafine particles due to the effect of canted or disordered spins at the particle surface [20]. The best fitting results are shown as solid lines in Fig. 4. From the fits, technical saturation magnetization M_s at different temperatures was derived. M_s is approximately 150 emu/g and 140 emu/g at 88 and 300 K, respectively. These values are equivalent to the values for Fe-Ni bulks samples reported in [23].

The magnetic coercivity H_c at different temperatures was determined from the low field part of the corresponding magnetization loop. The results of H_c vs. T are shown in Fig. 5. The coercivity value is very small, being 78 Oe at 88 K, and sharply decreases as temperature increases above room temperature. The coercivity can be originated from the interactions between the magnetic grains and the magnetic anisotropy induced by particle shape and surface.

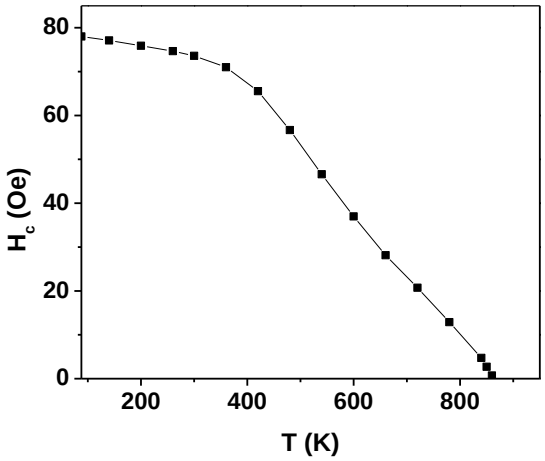

Figure 5. Magnetic coercive as a function of temperature.

Temperature dependence of the technical saturation magnetization of the samples is shown in Fig. 6. From the M_S–T curve, the Curie temperature T_C was determined to be 860 K. The spontaneous magnetization at 0 K $M_s(0)$ was estimated by extrapolation of the low-temperature part according to a modified Bloch equation $M_s(T) = M_s(0)*[1-B*T^{\alpha}]$ [24] where $M_s(0)$ is the spontaneous magnetization at 0 K, B and α are the Bloch constant and the Bloch exponent, respectively. A value of 152 emu/g is derived for $M_s(0)$.

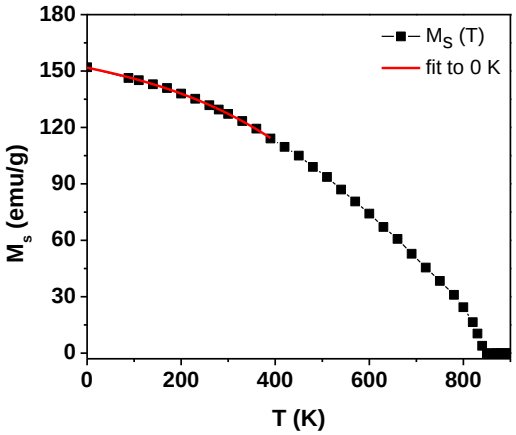

Figure 6. Spontaneous magnetization M_s as a function of temperature for the sample Fe-Ni alloy nanoparticles. The red lines are the fit curves according to the modified Bloch equation.

Figure 7 shows the magnetoresistance effect *MR* of the Fe-Ni nanoparticles. The observed results show that the sample resistance gradually decreases as the magnetic field increases. The

magnetoresistance effect is calculated as $MR = \{R(H)-R(0)\}/R(0)$ with $R(H)$ and $R(0)$ are the resistance in applied magnetic field H and in zero field, respectively. MR reaches 14% and 11.5% in 9.6 kOe at 88 and 300 K, respectively. The MR effect can be understood based on the tunneling process of electrons via the grain boundaries. This magneto transport behavior confirms the nanostructure of the Ni-Fe alloy sample.

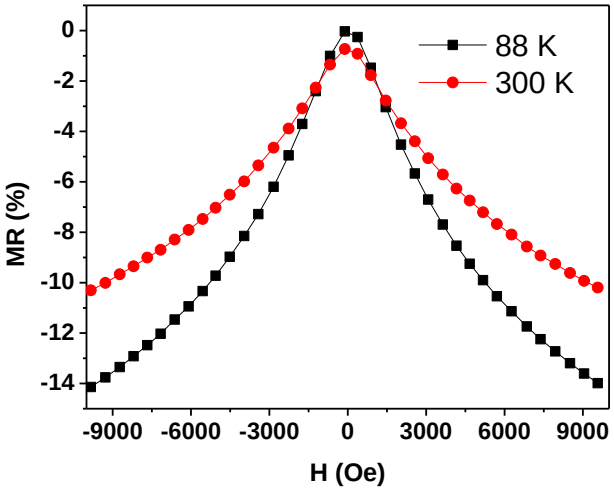

Figure 7. Magnetoresistance curves at 88 K and 300 K of Fe-Ni nanoparticles.

4. Conclusions

Fe-Ni nanoparticles were successfully synthesized from $NiFe_2O_4$ nanoparticles by deoxidizing in a reduced hydrogen atmosphere at elevated temperatures. The obtained results showed that the deoxidization time and temperature significantly affect the microstructure, morphologies, magnetic properties, and magnetoresistance of the samples. The air-annealed cubic $NiFe_2O_4$ ferrite could be firstly deoxidized into *bcc* Fe-Ni alloy, then transformed into *fcc* Fe-Ni alloy in hydrogen with the deoxidization temperature and deoxidization time. The Fe-Ni nanoparticles exhibit superparamagnetic behavior with high magnetization and high Curie temperature. These results showed that the Ni-Fe alloys prepared by thefabrication route can be prospected candidates for practical applications.

Acknowledgments.

This work was financially supported by the Vietnam National Foundation for Science and Technology Development under Grant No. 103.02-2019.321.

References

[1] K. Gheisari, S. Shahriari, S. Javadpour, Structural Evolution and Magnetic Properties of Nanocrystalline 50 Permalloy Powders Prepared by Mechanical Alloying, Journal of Alloys and Compounds, Vol. 574, 2013, pp. 71-82, https://doi.org/10.1016/j.jallcom.2013.03.277.

[2] Z. Liu, S. Li, Y. Yang, S. Peng, Z. Hu, Y. Qian, Complex-Surfactant-Assisted Hydrothermal Route to Ferromagnetic Nickel Nanobelts, Advanced Materials, Vol. 15, No. 22, 2003, pp. 1946-1948, https://doi.org/10.1002/adma.200305663.

[3] Z. Zhong, Y. Mastai, Y. Koltypin, Y. Zhao, A. Gedanken, Sonochemical Coating of Nanosized Nickel on Alumina Submicrospheres and the Interaction between the Nickel and Nickel Oxide with the Substrate, Chemistry Materials, Vol. 11, No. 9, 1999, pp. 2350-2359, https://doi.org/10.1021/cm981005m.

[4] I. Ban, M. Drofenik, D. Makovec, The Synthesis of Iron-Nickel Alloy Nanoparticles using A Reverse Micelle Technique, Journal of Magnetism and Magnetic Materials, Vol. 307, 2006, pp. 250-256, https://doi.org/10.1016/j.jmmm.2006.04.010.

[5] Y. J. Suh, H. D. Jang, H. Chang, W. B. Kim, H. C. Kim, Size-Controlled Synthesis of Fe–Ni Alloy Nanoparticles by Hydrogen Reduction of Metal Chlorides, Powder Technol, Vol. 161, No. 3, 2006, pp. 196-201, https://doi.org/ 10.1016/j.powtec.2005.11.002, 2006.

[6] R. D. Rutledge, W. H. Morris, M. S. Wellons, Z. Gai, J. Shen, J. Bentley, J. E. Wittig, C. M. Lukehart, Formation of FePt Nanoparticles Having High Coercivity, Journal of the American Chemical Society, Vol. 128, No. 44, 2006, pp. 14210-14211, https://doi.org/ 10.1021/ja0633868.

[7] M. Yamauchi, T. Tsukuda, Dalton Trans, Production of an Ordered (B2) CuPd Nanoalloy By Low-Temperature Annealing Under Hydrogen Atmosphere, Dalton Transactions, Vol. 40, 2011, pp. 4842-4845, https://doi.org/10.1039/C0DT01632B

[8] M. Yamauchi, R. Abe, T. Tsukuda, K. Kato, M. Takata, Highly Selective Ammonia Synthesis From Nitrate with Photo Catalytically Generated Hydrogen on CuPd/TiO_2, Journal of the American Chemical Society, Vol. 133, 2011, pp. 1150-1152, https://doi.org/10.1021/ja106285p.

[9] Q. L. Liao, R. Tannenbaum, Z. L. Wang, Synthesis of FeNi3 Alloyed Nanoparticles By Hydrothermal Reduction, The Journal of Physical Chemistry B, Vol. 110, No. 29, 2006, pp. 14262-14265, https://doi.org/10.1021/jp0625154.

[10] W. An, D. Gatewood, B. Dunlap, - C. H. Turner, Catalytic Activity of Bimetallic Nickel Alloys for Solid-Oxide Fuel Cell Anode Reactions from Density-Functional Theory, Journal of Power Sources, Vol. 196, 2011, pp. 4724-4728, https://doi.org/10.1016/j.jpowsour.2011.01.007.

[11] C. G. Zhang, J. J. Li, C. S. Shi, E. Z. Liu, X. W. Du, W. Feng, - N. Q. Zhao, The Efficient Synthesis of Carbon Nano-Onions Using Chemical Vapor Deposition on An Unsupported Ni–Fe Alloy Catalyst, Carbon, Vol. 49, No. 4, 2011, pp. 1151-1158, https://doi.org/10.1016/j.carbon.2010.11.030.

[12] O. Margeat, D. Ciuculescu, P. Lecante, M. Respaud, C. Amiens, B. Chaudret, NiFe Nanoparticles: A Soft Magnetic Material?, Small, Vol. 3, No. 3, 2007, pp. 451-458, https://doi.org/10.1002/smll.200600329.

[13] B. Folch, J. Larionova, Y. Guari, L. Datas, C. Guérin, A Coordination Polymer Precursor Approach to the Synthesis of Nife Bimetallic Nanoparticles Within Hybrid Mesoporous Silica, Journal of Materials Chemistry, Vol. 16, 2006, pp. 4435-4442, https://doi.org/10.1039/B608058H.

[14] J. M. Yan, X. B. Zhang, S. Han, H. Shioyama, Q. Xu, Magnetically Recyclable Fe–Ni Alloy Catalyzed Dehydrogenation of Ammonia Borane In Aqueous Solution Under Ambient Atmosphere, J. Power Sources, Vol. 194, No. 1, 2009, pp. 478-481, https://doi.org/10.1016/j.jpowsour.2009.04.023.

[15] S. A. Theofanidis, H. Poelman, G. B. Marin, V. V. Galvita, Enhanced Carbon-Resistant Dry Reforming Fe-Ni Catalyst: Role of Fe, ACS Catalysis, Vol. 5, No. 5, 2015, pp. 3028-3039, https://doi.org/10.1021/acscatal.5b00357.

[16] L. Wang, D. Li, M. Koike, S. Koso, Y. Nakagawa, Y. Xu, K. Tomishige, Catalytic Performance and Characterization of Ni-Fe Catalysts For The Steam Reforming of Tar From Biomass Pyrolysis to Synthesis Gas, Applied Catalysis A: General, Vol. 392, No. 1-2, 2011, pp. 248-255, https://doi.org/10.1016/j.apcata.2010.11.013.

[17] L. Wang, D. Li, M. Koike, H. Watanabe, Y. Nakagawa, Y. Xu, K. Tomishige, Catalytic Performance and Characterization of Ni-Co Catalysts for the Steam Reforming of Biomass Tar to Synthesis Gas, Fuel, Vol. 112, 2013, pp. 654-661, https://doi.org/10.1016/j.fuel.2012.01.073.

[18] S. A. Theofanidis, V. V. Galvita, M. Sabbe, H. Poelman, C. Detavernier, G. B. Marin, Controlling the Stability of A Fe–Ni Reforming Catalyst: Structural Organization of the Active Components, Applied Catalysis B: Environmental, Vol. 209, 2017, pp. 405-416, https://doi.org/10.1016/j.apcatb.2017.03.025.

[19] K. Tomishige, D. Li, M. Tamura, Y. Nakagawa, Nickel–Iron Alloy Catalysts for Reforming of Hydrocarbons: Preparation, Structure, and Catalytic Properties, Catalysis Science & Technology, Vol. 7, No. 18, 2017, pp. 3952-3979, https://doi.org/10.1039/C7CY01300K.

[20] L. N. Anh, T. T. Loan, N. P. Duong, S. Soontaranon, T. T. V. Nga, T. D. Hien, Influence of Y and La Substitution on Particle Size, Structural and Magnetic Properties of Nanosized Nickel Ferrite Prepared by Using Citrate Precursor Method, Journal of Alloys and Compounds, Vol. 647, 2015, pp. 419-426, https://doi.org/10.1016/j.jallcom.2015.04.240.

[21] B. Ravel, M. Newville, ATHENA, ARTEMIS, HEPHAESTUS: Data Analysis for X-Ray Absorption Spectroscopy Using IFEFFIT, Journal of Synchrotron Radiation, Vol. 12, 2005, pp. 537-41, https://doi.org/10.1107/S0909049505012719.

[22] R. M. Bozorth, J. G. Walker, Magnetic Crystal Anisotropy and Magnetostriction of Iron-Nickel Alloys, Physical Review, Vol. 89, No. 3, 1953, pp. 624-628, https://doi.org/10.1103/PhysRev.89.624.

[23] K. S. Dijith, R. Aiswaryaa, M. Praveena, S. Pillai, K. P. Surendran, Polyol Derived Ni and Nife Alloys For Effective Shielding of Electromagnetic Interference, Materials Chemistry Frontiers, Vol. 2, 2018, pp. 1829-1841, https://doi.org/10.1039/C8QM00264A.

[24] S. Linderoth, L. Balcells, A. Labarta, J. Tejada, P. V. Hendriksen, S. A. Sethi, Magnetization and Mössbauer Studies of Ultrafine Fe-C Particles, Journal of Magnetism and Magnetic Materials, Vol. 124, 1993, pp. 269-276, https://doi.org/10.1016/0304-8853(93)90125-L.